Lund University

Bachelor Thesis in Physics

Sensitivity of various qubit detection methods in Pr:Y_2SiO_5

Vassily Kornienko

Supervisor: Stefan Kröll
Co-Supervisor: Adam Kinos

Lund University
Faculty of Science

Department of Atomic Physics

Hand-in date: May 5th 2017
Project Duration: January 2017 - May 2017

Popular Science Article

Imagine a room where there is one door where you can enter and two doors where you can exit. In each room there is a set of instructions related to if you feel hot or cold. If you feel hot you might have to go through the left door while if you feel cold you might have to go through the right door. There can also be rooms where there is a fireplace, so if you are hot you will just get hotter while if you are cold you warm up. The opposite could be achieved by installing an air conditioner. Now imagine another set of rooms where two people can enter and there are three door where one can exit. The instructions could look like this:

1. If you are both hot one of you should go through the leftmost door.

2. If you are both cold one of you should go through the rightmost door.

3. If one of you is hot and the other one is cold the hot person should go through the middle door.

By interchanging hot and cold with a 1 and a 0, the above thought experiment is in direct analogy with a normal computer. The people that are in this maze of rooms are the so-called bits (of which eight make up a byte), and the instructions in every room are put there by the programmers.

If we stay along the lines of this thought experiment, what if one could use the broader sense of hot and cold that humans can feel. For example you could be freezing, cold hands but warm body, both hot and cold because you have contracted a fever or just on the verge of breaking a sweat. This is what the next generation of computers, called quantum computers, will be able to do. These computers will be able to use and control the infinite amount of data that is stored in nature itself without ever having to access it. Many new strange phenomena can also be accessed such as a process called entanglement. This will allow the programmers to control each person in the maze by only controlling one of them. The great science fiction dream of teleportation is also a possibility in this new maze. Everything sounds promising so far, the catch is that that in order for the programmers to be able to use all these new tools, the maze has to be very well isolated from the outside world. The way to solve this is to put it in a building made out of thick slabs of lead.

This isolated building does not seem too bad as long as the set of instructions is put in before the people start walking through the maze. When everybody comes out of the other end, the sequence of hots and colds that they represent will be the answer to what the programmers asked, however there is a thick slab of lead between the two. How does the programmer access the answer? This is the problem that this bachelor thesis addresses.

The type of maze or quantum computer hardware that Lund is investigating uses laser light to give the instructions to atoms that are stuck inside a larger structure, a crystal. Since the number of atoms in this crystal is very low the signals that come from them will be very faint. In the maze analogy the low number of atoms protected by the crystal corresponds to the slab of lead. Hence a new way of reading these signals in a reliable manner has been proposed and investigated in this thesis.

Abstract

The long coherence times of the 4f hyperfine levels of rare-earth-ions gives the possibility to use these as quantum computation devices. Moreover after being doped into a crystal the strong dipole-dipole interaction can be utilized to entangle them. Much work has been done here in Lund to attain as many of the DiVincenzo criteria as possible. At the moment work is being done in the creation of a multiple qubit gate, namely the controlled NOT gate. However, due to an exponential decay in the probability of attaining this gate with respect to the number of involved qubits, along with the low doping concentration, the number of atoms that take part in these gates will be very small. Detecting the signal from such a small population is problematic. This thesis addresses this problem by comparing the established readout method that consists of a simple scan, with two new readout methods: a slow scan, i.e., a scan with low frequency chirp and a method called superposition beating which incorporates the fundamentals of heterodyne detection with the free induction decay of an ensemble of atoms. A way of calculating the signal to background ratio in order to maximize the existing signal is also proposed and investigated. The results are then compared to Bloch simulations to give a more intuitive grasp of the quantities that are being discussed. Using the superposition beating method 7% of the maximum qubit population could be detected. Furthermore a population resolution of 2 percentage points was achieved.

Contents

1 Introduction

The use of quantum mechanisms is what makes quantum computing considerably more efficient than classical computing at some specific problems. These mechanisms include entanglement, superposition states, and arbitrary unitary transformations, of which the latter greatly increases the variety of operations that can be performed beyond the classical logic gates. Exponential speed up can be achieved for Fourier transforms and large number factorization, an algorithm discovered by Peter Shor, while Grover's search algorithm provides a square-root speed up in the traveling salesman problem [1]. Furthermore, as thoroughly described on pages 204-212 of [2], a quantum simulation algorithm that can efficiently solve the time-dependent Schrödinger equation for a large variety of Hamiltonians can be implemented.

In order to perform these algorithms IBM's David P. DiVincenzo made a list of criteria that must be met by any physical realization of a quantum computer [3]. The list includes the requirement that it must be possible to prepare the individual entities, qubits, in precise ways followed by the ability to perform a universal set of unitary transformations. When it comes to actually achieving this experimentally, the balance between preserving the quantumness of the system while still requiring it to interact strongly with neighbouring systems, poses strong restraints on the type of scheme that can be used. As of today superconducting qubits and ion traps have come the farthest, while new ideas such as majorana qubits are being proposed.

Rare-earth-ion doped crystals are also a good candidate. High fidelity qubits have been created by using the interaction of hyperfine energy levels with coherent light [4]. Along with the dipole-dipole interaction between individual ions, these crystals have the potential of becoming good quantum computing hardware.

Similar to bits in classical computers, the result of all these gate transformations must be read in an efficient manner and measuring quantum systems poses problems of its own. The small population of ions in these crystals cause the absorption signal to be very faint. Therefore a new method for reading out the state of a qubit in rare-earth-ion doped crystals will be proposed and analyzed in this thesis.

2 Theory

In order to achieve an efficient readout method, knowledge from various fields of physics is needed. The essentials are presented in the following section.

2.1 The crystal

Due to the shielding provided by the 5s and 5p shells, the 4f optical transitions of rare earth elements, also known as lanthanides, are long lived. The lifetimes usually range from microseconds to milliseconds but can reach days for some transitions, a considerable duration in atomic physics. These long lifetimes, or coherence times, along with the short laser pulses used to perform operations, give rise to the possibility of attaining the threshold of 10^4 logic operations before coherence is lost. This is a threshold that is essential to pass in order to be able to handle quantum noise, pages 481-484 of [2]. Therefore these optical transitions in lanthanides seem to be viable candidates for qubits.

The specific crystal used for these experiments is yttrium orthosilicate, Y_2SiO_5, doped with praseodymium ions at a concentration of 0.05%. When doped into the crystal the optical properties of these triply ionized atoms will be comparable to the optical properties of a gas consisting of identical atoms [5]. As a result of the random doping and the larger radius of the praseodymium ions as compared to the yttrium ions which it replaces, each ion will "see" a different electrical surrounding. This lack of symmetry will shift the aforementioned energy levels of each ion differently, creating a 9GHz wide, inhomogenously broadened spectral line centered at 606nm. As shown in figure 1, this line is the sum of the homogenously broadened lines of each ion. Additionally, the number of ions that "see" identical surroundings, referred to as an ensemble, will determine the amplitude of the absorption line.

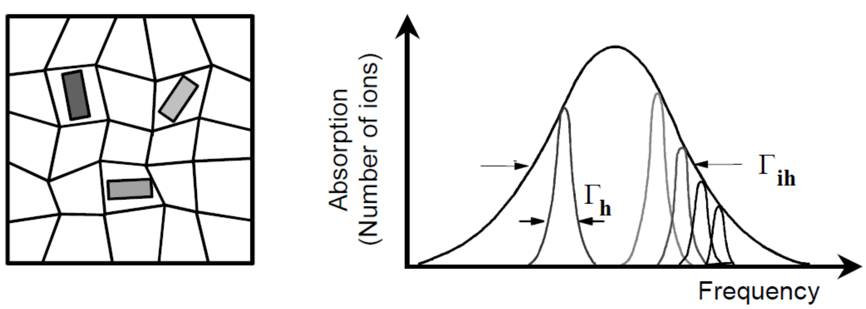

Figure 1: The left figure shows how the ions will "see" different electrical surroundings, while the right figure shows the effect that this has on the absorption spectrum. The inhomogenous line is the sum of the homogenous lines of all ions. Figure adopted from [5].

2.2 Energy level structure

The 4f hyperfine energy level structure that is utilized consists of three ground hyperfine levels and three excited hyperfine levels, see figure 2. The kets to the right of each level represent the qubit states. This ket nomenclature is more in tune with the quantum computation perspective than the LS-coupling classification system, however the two will be interchanged freely according to appropriateness. The oscillator strengths of Table 1 are the probabilities that a given excited state will decay directly to a given ground state via the electric dipole interaction. This is directly related to the dipole matrix element, $\langle g| \hat{e} \cdot \hat{r} |e\rangle$, between the two levels.

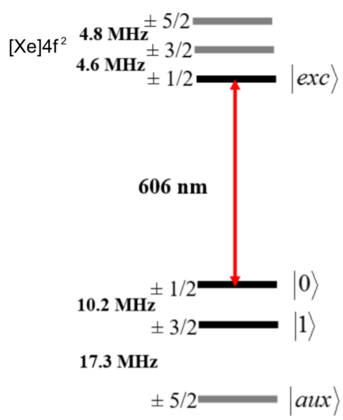

Figure 2: 4f hyperfine energy level diagram.

g\e	± 1/2	± 3/2	± 5/2
± 1/2	0.55	0.38	0.06
± 3/2	0.39	0.60	0.01
± 5/2	0.05	0.02	0.93

Table 1: Oscillator strength [arb. units].

As mentioned earlier, the lifetimes of the excited hyperfine levels are of the order of a hundred microseconds while the relaxation times of the $|0\rangle$, $|1\rangle$ and $|aux\rangle$ states are of the order of milliseconds. These ground state lifetimes can however be extended to seconds upon the application of appropriate magnetic fields [5].

2.3 Interaction of light with matter

A prerequisite to being able to control the state of the qubits optically, is an understanding of how coherent light interacts with them. This intuitive understanding can be reached by introducing the Bloch formalism, presented in this section.

A two level problem

Consider a two energy level system. The rotating wave approximation states that a large detuning of a photon from the resonance energy of the transition will have a negligible effect on the system, page 125 of [6]. Therefore, as long as we can neglect decay to other levels, i.e., the pulse durations are much shorter than the lifetimes, it is sufficient to describe the interaction of light with the energy level system of figure 2 as a set of separate two level systems. This simplifies the problem considerably.

Bloch equations

Assuming that the coherence time is lifetime limited, the time-dependent Schrödinger equation describing the interaction of a two level quantum mechanical system with a classical electromagnetic wave, can be rewritten into the Bloch equations as follows,

$$\dot{u} = -\frac{\Gamma}{2}u + \delta v + \Omega_{im} w, \tag{1}$$

$$\dot{v} = -\delta u - \frac{\Gamma}{2}v + \Omega_{re} w, \tag{2}$$

$$\dot{w} = -\Omega_{im} u - \Omega_{re} v - \Gamma(w+1), \tag{3}$$

where Γ is the inverse of the lifetime and δ is the detuning of the electromagnetic wave (ω) from the resonant frequency of the transition (ω_0), $\delta = \omega_0 - \omega$, page 137 of [6]. The letters u, v and w are the components of the system's state vector, in its corresponding 3 dimensional Hilbert space. A thorough explanation of this concept will be given in the next section. Ω is the Rabi frequency, given by:

$$\Omega = \frac{\langle g| \hat{r} |e\rangle}{\hbar} eE_0 = \frac{X_{12}}{\hbar} eE_0 \tag{4}$$

where X_{12} is the dipole matrix element between the ground state $|g\rangle$ and excited state $|e\rangle$, e is the elementary charge, E_0 is the electric field amplitude of the interacting electromagnetic wave and $\hbar$ is the reduced Planck constant. From equation 4 it is seen that the light intensity I is proportional to the rabi frequency squared, $I \propto |\Omega|^2$, hence the Rabi frequency can be interpreted as a measure of the intensity of the wave, scaled with respect to the oscillator strength of the given transition. In other words it is a measure of how efficiently an electromagnetic wave of fixed intensity will interact with the transition. Note also that, in accordance to the so-called rotating wave approximation, δ is small compared to the frequency separation of the two levels.

Bloch Sphere

If an orthonormal basis, $(\hat{e}_x, \hat{e}_y, \hat{e}_z)$, and a vector $\vec{R} = (u, v, w)$ (the same u, v, and w of equations 1, 2 and 3) is introduced, it can be shown that $|\vec{R}| = 1$. This can further be developed to show that the Bloch equations are actually equations of quantum motion, describing the movement of a quantum state, $\vec{R}$, along the surface of a unit sphere, the Bloch sphere, pages 128-131 of [6]. Defining a vector of motion as $\vec{W} = (-\Omega_{re}\hat{e}_x, \Omega_{im}\hat{e}_y, -\delta\hat{e}_z)$, where the subscripts im and re are given to represent the real and imaginary part of the Rabi frequency respectively, the Bloch equations can be rewritten in vector form as

$$\dot{\vec{R}} = \vec{W} \times \vec{R}. \tag{5}$$

Equation 5 means that the state vector $\vec{R}$ will precess around the driving vector $\vec{W}$ at a speed characterized by $\sqrt{\Omega_{re}^2 + \Omega_{im}^2 + \delta^2}$.

This Bloch sphere is a subspace of a Hilbert space, and each point on its surface corresponds to a unique quantum state. Special states include the poles along $\hat{e}_z$ which correspond to the energy eigenstates of the system, and the poles along the $\hat{e}_y$ and $\hat{e_x}$ axes which correspond to real and imaginary orthogonal 50/50 superposition states respectively. This is shown in figure 3.

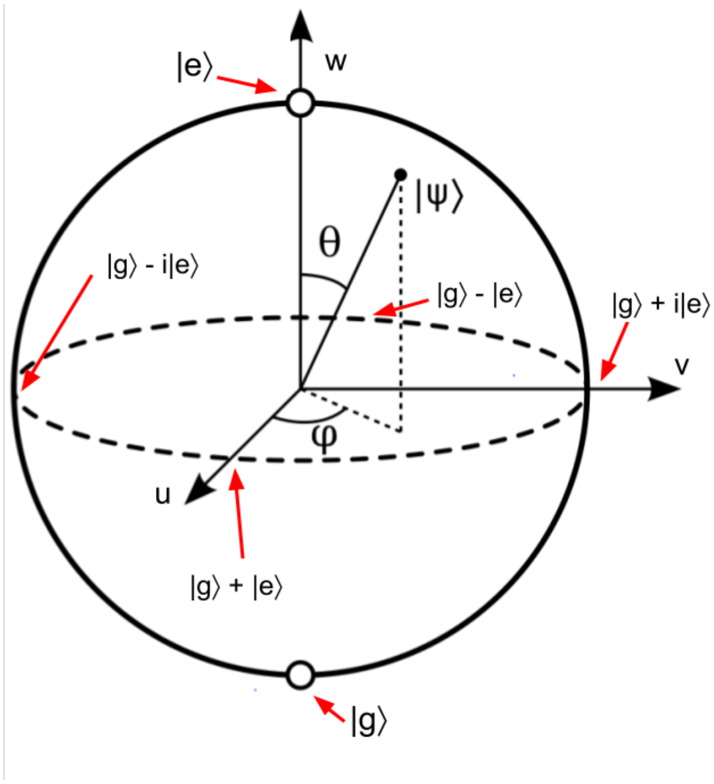

Figure 3: The Bloch sphere as described in the text. The red arrows correspond to various states along the basis axes and $|\Psi\rangle$ is an arbitrary quantum state, given by a unique $\vec{R}$. The normalization factor of $\frac{1}{\sqrt{2}}$ has been omitted for clarity. Figure adapted from [7].

This way of visualizing a two level quantum system gives an intuitive understanding of how an electromagnetic wave interacts with a qubit. Along the course of this thesis, Bloch formalism will allow us to make simple predictions of how our qubits evolve in time.

Electromagnetic pulses

Since the entries of the $\vec{W}$ vector correspond to the parameters of the interacting electromagnetic wave, varying the intensity, duration, central frequency and frequency chirp in experimental situations can give us fine control over the state vector, $\vec{R}$, of the system. Numerically solving the Bloch equations, so called performing Bloch simulations, is an important tool used to investigate how varying the parameters of the electromagnetic wave changes the evolution of the system in time.

Figure 4(a) shows how a square pulse with no frequency chirp, no detuning and a fixed top hat intensity distribution in the time domain, will cause the atom to so called, rabi oscillate. In the Bloch sphere picture the driving vector, $\vec{W}$, points in the negative u direction and the state vector $\vec{R}$ will rotate along the v-w plane. Motivated by the oscillatory structure of the interaction, so called π and $\pi/2$ pulses are defined. These are given as the square pulse durations that rotate the system's state vector by 180° or 90° respectively. For example a π-pulse will move a qubit from its ground state to a 100% excited state and a $\pi/2$-pulse will move a qubit from the ground state to a 50/50 superposition state.

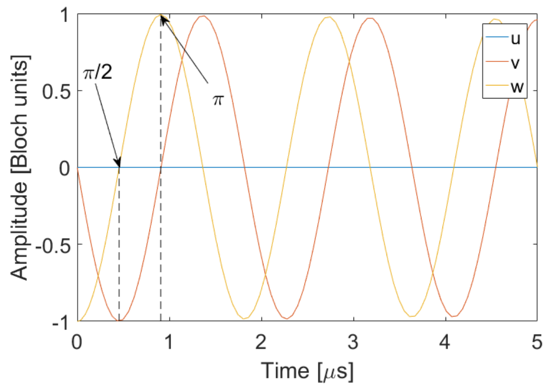

(a) Square pulse

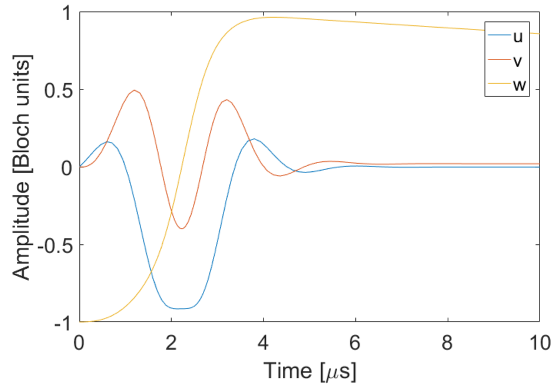

(b) Sechyp pulse

Figure 4: Bloch simulations for two types of pulses, the square and sechyp pulse. The π and $\pi/2$ pulse times of the square pulse are included. The damping of the rabi oscillations and the decay of the population in the sechyp simulation are caused by a non-zero Γ. Bloch units are simply the coordinates that the vector has in the relevant axis. For example when $w = -1$, the system is in the ground state and when $w = 0$ the system is in a 50/50 superposition.

It turns out that the effect of these square pulses on the system will be sensitive to the intensity and detuning of the pulse [4]. Therefore, in experimental situations where the laser intensity fluctuates and full control over the qubits is desired, the sechyp pulse is used. This pulse has the following form:

$$\Omega = \Omega_0 \mathrm{sech}\big(\beta(t - t_0)\big)^{(1-i\mu)} \tag{6}$$

where μ and β are related to the frequency chirp and full width half maximum time of the pulse, Ω_0 is the rabi frequency amplitude of the pulse and t_0 is the central time of the pulse. Bloch simulations of this pulse were performed in figure 4(b) showing that β and μ have been chosen so as to not affect the atoms after they have been fully excited (the decrease is caused by the lifetime of the level). In contrast to the square pulse high robustness against intensity fluctuations and detuning of the sechyp pulse have been shown [4]. This gives the possibility of very fine control of the state vector, $\vec{R}$, and the size of the affected population.

2.4 Free Induction Decay

Free induction decay is the emission of fluorescent light due to an arbitrary excitation between two levels. Without loss of generality a 50/50 superposition state between a ground state, $|g\rangle$, and an excited state, $|e\rangle$, is examined. At time $t = 0$ a laser pulse is applied to the system creating the aforementioned superposition. This gives the total wavefunction

$$|\psi(0)\rangle = \frac{1}{\sqrt{2}}\big(\,|g\rangle + |e\rangle\,\big). \tag{7}$$

Assuming that the ground state has an infinite lifetime and after neglecting the global phase, the time dependent wavefunction for $t > 0$ will have the following form

$$|\psi(t)\rangle = |g\rangle + |e\rangle \exp\Big(-i\frac{E_{eg}t}{\hbar}\Big)\exp\Big(-\frac{t}{2\tau_e}\Big), \tag{8}$$

where τ_e is the lifetime of the excited state and E_{eg} is the energy difference between the ground and excited state. The time dependent intensity of the fluorescent light is

$$I(t) = A\Big|\,\langle g|\,\hat{e}\cdot\hat{r}\,|\psi(t)\rangle\,\Big|^2 \tag{9}$$

for some constant A and where $\hat{e}\cdot\hat{r}$ is the dipole operator [8]. Inserting equation 8 into equation 9 gives,

$$\begin{aligned} I(t) &= A\Bigg|\,\langle g|\,\hat{e}\cdot\hat{r}\Big[\,|g\rangle + |e\rangle \exp\Big(-i\frac{E_{eg}t}{\hbar}\Big)\exp\Big(-\frac{t}{2\tau_e}\Big)\Big]\Bigg|^2 \\ &= A\Bigg|\,\underbrace{\langle g|\,\hat{e}\cdot\hat{r}\,|g\rangle}_{=0} + \underbrace{\langle g|\,\hat{e}\cdot\hat{r}\,|e\rangle}_{\neq 0}\exp\Big(-i\frac{E_{eg}t}{\hbar}\Big)\exp\Big(-\frac{t}{2\tau_e}\Big)\Bigg|^2 \\ &= A\Big|\,\langle g|\,\hat{e}\cdot\hat{r}\,|e\rangle\,\Big|^2 \exp\Big(-\frac{t}{\tau_e}\Big). \end{aligned} \tag{10}$$

Equation (10) shows that there will be a non-zero fluorescent intensity which will decay exponentially depending on the lifetime of the excited state. In fact, since the values of Table 1 are directly related to the dipole matrix element, the intensity of equation 10 will scale in the same manner with respect to the levels considered.

Free induction decay of an ensemble of atoms

When one moves a whole ensemble of atoms to the north pole of the Bloch sphere, i.e., the excited state, each atom will start emitting light in the same manner as equation 10. However, their path to the south pole is completely random, so each atom will emit light with a different phase, in other words their emission will be incoherent. The interference of all these waves will cause the light to be of lower intensity than if they were all emitted coherently. More generally, in order to maximize the intensity, i.e., making sure the phase of each atom is identical, the projection of the state vector on the equatorial plane of the Bloch sphere should be maximized.

2.5 Beating

The law of superposition dictates how multiple classical waves will interact when their paths coincide. Consider two waves, of frequency ω_1 and ω_2 and phase difference ϕ following the same path. Then the total, superimposed wave will be

$$u = a_1\cos(\omega_1 t) + a_2\cos(\omega_2 t + \phi) = (a_1 + a_2)\cos\Big(\frac{\omega_1+\omega_2}{2}t + \frac{\phi}{2}\Big)\cos\Big(\frac{\omega_1-\omega_2}{2}t - \frac{\phi}{2}\Big), \tag{11}$$

where a_1 and a_2 are complex amplitudes. Since $\omega_1+\omega_2$ will oscillate very quickly, the $\omega_1-\omega_2$ term will be seen as the envelope of the superimposed wave. Squaring the amplitude will multiply the argument by two meaning that the beat frequency will be given by $\omega_{beat} = \omega_1 - \omega_2$.

Beating as a method of detection

Consider a system that emits light at a frequency ω_{ge}, and the intensity decays as in equation 10. If one sends a laser pulse of constant intensity I_l at frequency $\omega_l \neq \omega_{ge}$, the two will interfere as in equation 11. This means that a signal oscillating at frequency $\omega_l - \omega_{ge}$ with an envelope which decays exponentially to I_l can be detected. More generally the mixing of two frequencies followed by the detection of the beating pattern is commonly used for low-noise signal recovery, pages 407-408 in [8]. Using equation 11 and some trigonometric identities, the amplitude of the recorded signal in heterodyne detection, as this method is called, will be:

$$I = |A_{ge}\cos(\omega_{ge}t) + A_l\cos(\omega_l t)|^2 = A_{ge}A_l\cos(\omega_{beat}t) + \text{faster oscillating terms} \tag{12}$$

where the subscript ge is dedicated to the emitted light and the subscript l is dedicated to the laser. From equation 12 it can be seen that the signal can be amplified simply by increasing the intensity of the laser. This allows for control of the signal to noise ratio of a very weak signal.

2.6 Signal to Noise/Signal to Backgroud

The signal to noise ratio, SNR, is defined as the ratio between the signal level and noise level of a given spectrum. It is calculated by taking the amplitude of the signal, i.e., the height minus the zero level of the signal, divided by the amplitude of the noise in the signal's vicinity. This measure is dependent on where on the spectrum these two values are to be measured. If the location of the signal and other structures on the spectrum is well known, the SNR is a good measure.

If the exact structure of a spectrum is not known, a more robust measure must be devised. It will be called the SBR, short for signal to background ratio. Two ways of calculating this was used. The initial version was to integrate over the interesting signal of a given spectrum and divide that value by an integration of an equally sized domain in its vicinity. Note that these two values come from the same spectrum.

The second way of calculating the SBR was by integrating over a given domain on the zero signal spectrum and saving that value as S_0. Integration over the same domain of any other spectrum, S_s, is then divided by S_0. With this method a zero signal will give an SBR of 1 (S_0/S_0), and any signal that is even slightly above the noise, i.e., $S_s > S_0$, will be detected. Furthermore this method has the advantage of being objective to the choice of domain, since anything that is part of a recurring structure will automatically be compensated for, as long as it does not grow with signal strength.

3 Methodology

This section will present the method and setup that was used to, as efficiently as possible, proceed with the investigations.

3.1 Setup

Figure 5 shows the experimental setup. A CW Coherent 699-21 dye laser, lasing at 605.977nm with a linewidth of about 1MHz and an output power of around 400mW, is pumped by a 6W, 532nm Nd:YVO_4 Coherent Verdi-V6. This linewidth is too broad for these experiments so the laser frequency is stabilized using a vacuum-suspended high-finesse cavity, with free spectral range of 3GHz. This cavity measures the frequency error from the laser and feeds counteracting signals to an intracavity electro-optical modulator. This way the linewidth of the laser is decreased to the vicinity of 10Hz.

The light then enters a modulator setup where, using a bowtie mirror configuration, it passes through an acousto-optical modulator (AA optoelectronic model AA.ST.200/B100/A0.5-vis) twice. With a MATLAB controlled arbitrary waveform generator, which feeds the acousto-optical modulator with signals, the experimentalist has the freedom to create light pulses of arbitrarily chosen phase, amplitude and frequency patterns. This can be done efficiently down to a time resolution of 4ns, very low amplitudes and over a range of 200MHz. In order to clean the spatial mode of the beam and prevent beam walking, the light is then passed through a single mode fiber to the experimental table.

Once on the experimental table, the light is split by a beamsplitter into a reference and experimental beam. After being reflected by some mirrors, the experimental beam is focused using a 350mm lens onto the crystal sample, which itself is situated in a vacuum sealed helium bath cryostat, keeping it at a temperature of about 2.2K. In order to increase absorption, it is mounted in such a way that a vertical polarization of our beam is along the D2-axis of the crystal and the beam propagates along the b-axis. A typical power of the beam when it hits the crystal is 30mW, leading to an intensity of about $8 \times 10^7 \mathrm{W/m^2}$ when focused to a beam spot of $4 \times 10^{-10} \mathrm{m}^2$.

After being transmitted through the sample, the beam is focused on a Thorlabs PDB150A detector, which is of exactly the same model as the reference detector. These detectors are then connected to a Lecroy digital oscilloscope, and various MATLAB scripts process and plot the recorded data.

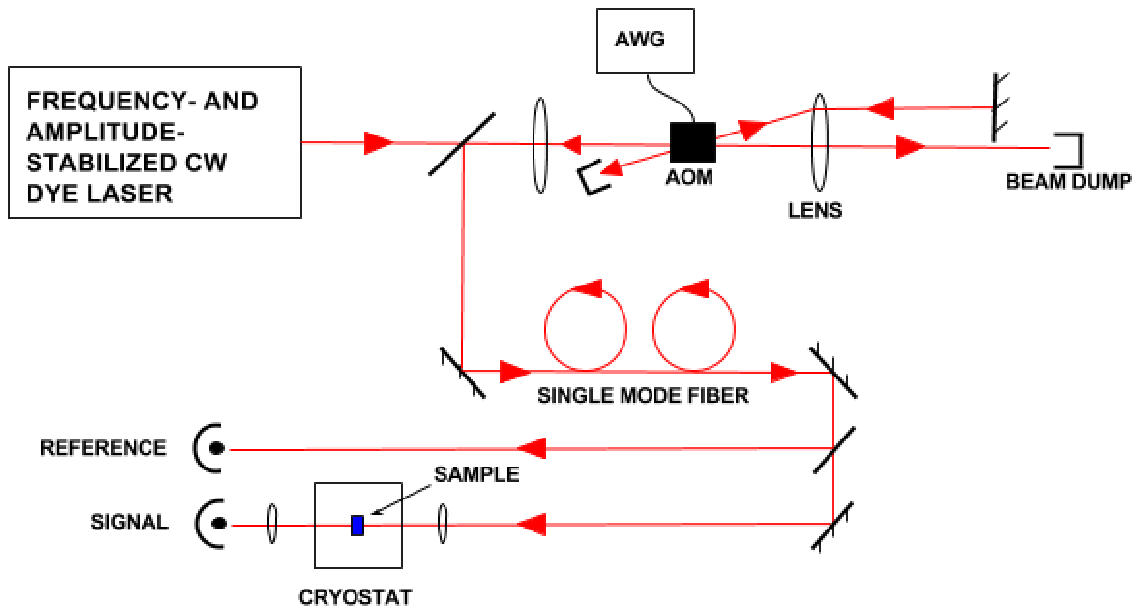

Figure 5: A schematic of the experimental setup used for the experiments. Details may be read in section 3.1.

3.2 Control and readout of the qubits

The qubits are ensembles of atoms that lie in the inhomogenous line profile of figure 1. Their preparation has been thoroughly investigated [4, 5] so a summary of the way this is done, followed by the currently used qubit readout method is included in this section.

Creation of the pit

Manipulating qubits efficiently using the absorption and emission of coherent light requires clearing the surrounding frequency domain from any other absorbing ions. The implementation of up to 600 separate pulses burns a 17MHz wide pit of little to no absorption in the inhomogenous line profile of figure 1 [5]. This size will be able to include all the relevant energy levels of figure 2. The burning process will moves the qubits into the $|5/2g\rangle$ state while moving the remaining ions to either the $|1/2g\rangle$ or $|3/2g\rangle$ state. Figure 6 is a readout scan of this burnt pit.

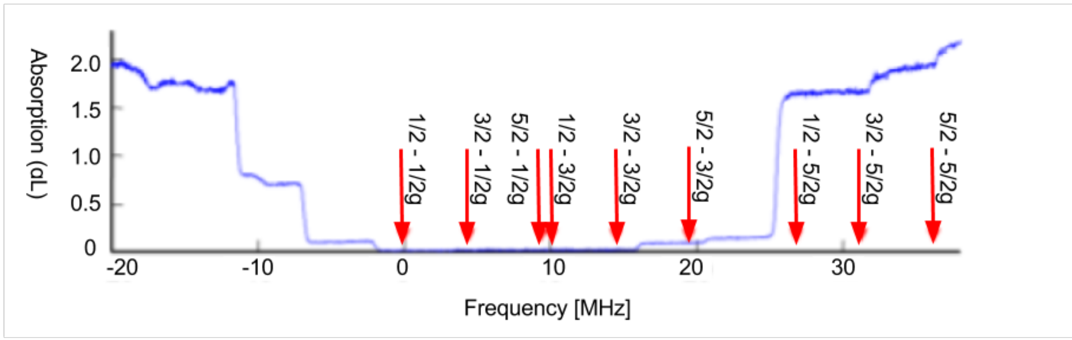

Figure 6: A figure of the pit, created in the inhomogenous profile. The arrows correspond to the position of the various transitions where the x-axis has been shifted so that the $1/2g - 1/2e$ transition is at 0MHz [9].

Creating the qubit

In order to create a qubit an ensemble of ions are moved to an energy level such that they absorb within the frequency range of the pit. This is done using a sequence of sechyp pulses, bringing ions from somewhere of high absorption to either the $|0\rangle$ or $|1\rangle$ level. In our protocol, the ions that have been moved to the $|5/2g\rangle$ level, are excited to the $|5/2e\rangle$, then immediately stimulated down to the $|1/2g\rangle$ energy level. The rabi frequency of the sechyp pulse moving the ions from $|5/2g\rangle$ to $|5/2e\rangle$ is denoted f_{trans}. Referring back to the theory on sechyp pulses of section 2.3, the absolute size of f_{trans} (where $\Omega_0 = 2\pi f_{trans}$) will determine the fraction of the population that is affected, albeit non-linearly.

3.3 Normal readout scan

The readout of the qubit has hitherto been performed by simply scanning across the pit with a square pulse of chirp rate 1MHz/s and rabi frequency of 80kHz. These values correspond to a sweet spot so that one does not start affecting the qubit too early in the scan but still have a decently sized absorption peak. In order to compensate for the phenomenon of coherent beating a deconvolution algorithm is required [10], giving a readout that looks like figure 7. There are three peaks, corresponding to the excitation of the ion ensemble to one of the three excited hyperfine levels respectively. Since the excitations caused by the scan itself are assumed to be small, the size of the peaks will mainly depend on the differing oscillator strengths of Table 1. However if a scan of an excited state is to be made, the lifetime will be a considerable source of error (the scan takes 30μs while an excited state lifetime is around 160μs). In contrast, because of the slow hyperfine level relaxation, the lifetimes will not be of importance when scans over ground states are performed.

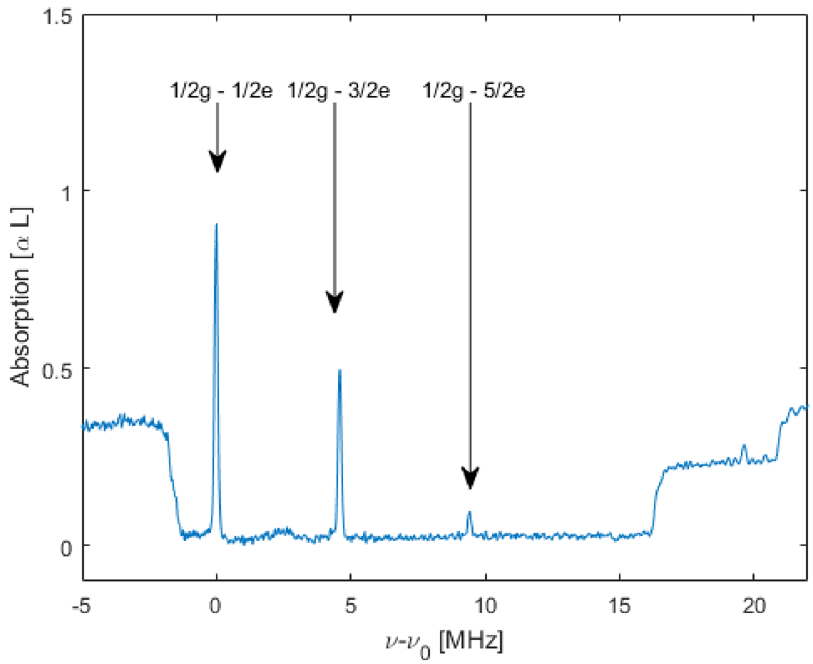

Figure 7: A normal readout scan of a qubit in the $|0\rangle$ state. The three peaks correspond to the three possible excitations, matching with the energy splittings of figure 2. The positions of the peaks are identical to their positions in figure 6.

3.4 General method

The aim of this project is to devise a new way of detecting the signal from a small population in the emptied pit. Therefore, after the pit has been created, the general method will be to vary the population size of $|0\rangle$ by varying the size of f_{trans} (this correspondence will be empirically shown in the results section). The different readout methods will then be tested for these different peak sizes. Ten readouts will be performed for every change of parameters so that a mean and standard error of the mean can be extracted. The laser fluctuations will be taken care of by dividing the signal by the reference for each run. Since the emphasis of this thesis is to try many different cases and methods, this was considered the optimum trade-off between the precision of results and the time it would take. When it comes to error analyses, the standard error of the mean will be plotted. This since if a qubit is in the state $|\psi\rangle = \alpha\,|0\rangle + \beta\,|1\rangle$, one will have to perform many measurements in order to determine α and β. Hence shot to shot noise is not as relevant as the mean. Moreover, we are not currently trying to minimize shot to shot variations.

3.5 Readout methods

Two readout methods beyond the normal readout scan are to be tested, namely a slow readout scan and a method we call superposition beating.

Slow readout scan over a small frequency range

Since it is known where the ions should be, trying to scan over a small frequency range while varying chirp rate and rabi frequency has the potential of giving a better SBR. The type of pulse used here will be a square pulse, with a rabi frequency given by f_{read}.

Superposition beating

Using the free induction decay of a superposition state along with incoming laser light at a different frequency, a heterodyne detection scheme can be established. The procedure is to combine the ideas of sections 2.4 and 2.5 by creating a 50/50 superposition between the $|0\rangle$ state and any of the excited states followed immediately by a square readout pulse at frequency $\omega_l \neq \omega_{1/2g-exc}$. Hence if there is a non-zero population in the $|0\rangle$ state, the detected signal will oscillate at $\omega_{beat} = \omega_l - \omega_{1/2g-exc}$. Performing a Fourier transform of this signal will give rise to a peak at ω_{beat}.

The key to this method is the creation of a 50/50 superposition of states. Since we are working with very low absorption coefficients (of the order of 0.1m^{-1}), it is essential to get as much light out of the system as possible. Therefore a 50/50 superposition, where all ions decay with the same phase, is preferred.

Various parameters will be changed in order to characterize the peak at ω_{beat}. These include the rabi frequency of the readout signal, f_{read}, the choice of level to create the superposition with, the frequency shift of the readout pulse, ω_{beat}, and duration of the readout pulse.

4 Results

The following section presents the results of the investigations.

4.1 Initial tests for all three methods

All three methods

In order to obtain an initial intuition of how well they perform, all three methods were tested for various populations in the $|0\rangle$ level, and are presented in figure 8. These populations were seen to be dictated by the rabi frequency of the $5/2g - 5/2e$ pulse, f_{trans} (see section 3.2). The beat signal, ω_{beat}, was set at 1MHz.

The units on the x-axes of the normal and slow readout of figure 8 are given as the transition frequency, shifted such that zero corresponds to the $1/2g - 1/2e$ transition. The unit of the x-axis of the beating method, is the frequency of a given Fourier component of the signal. In other words, the normal and slow readouts are in time space while the beating readout is in frequency space.

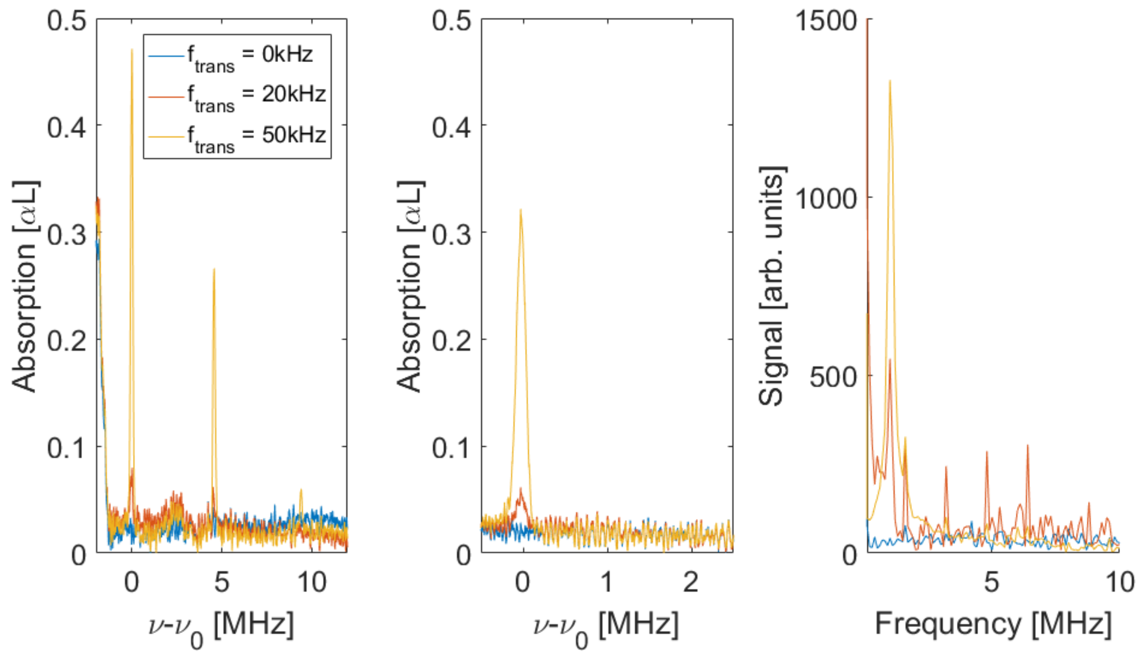

Figure 8: From left to right: the signals using the normal readout method, the slow readout method and the superposition beating method for various f_{trans}.

Upon comparison of the slow readout method and beating method with both figure 7 and the first plot of figure 8, one can observe qualitative and quantitative differences. Without ambiguity one can see from the blue lines of figure 8 that when there is not supposed to be a peak, none of the methods will show one. As f_{trans} increases, a peak will be visible in all three methods, however a small bump will appear in the normal readout and a lot of noise in the form of harmonics and unwanted frequencies will be introduced to the spectrum of the superposition beating method. The reason for this small bump in the normal readout method is unknown, however it has never been seen in prior or current measurements. Therefore it is assumed to be some abnormality related to this set of experiments. At large f_{trans} there is no doubt that the peaks will be visible for all methods, seen as the yellow line in figure 8.

Quantifying peak size

To better understand which method works well for different f_{trans}, figure 9 plots of the SNR of each method as a function of f_{trans} (defined in section 3.2). The standard error of the mean is given as errorbars.

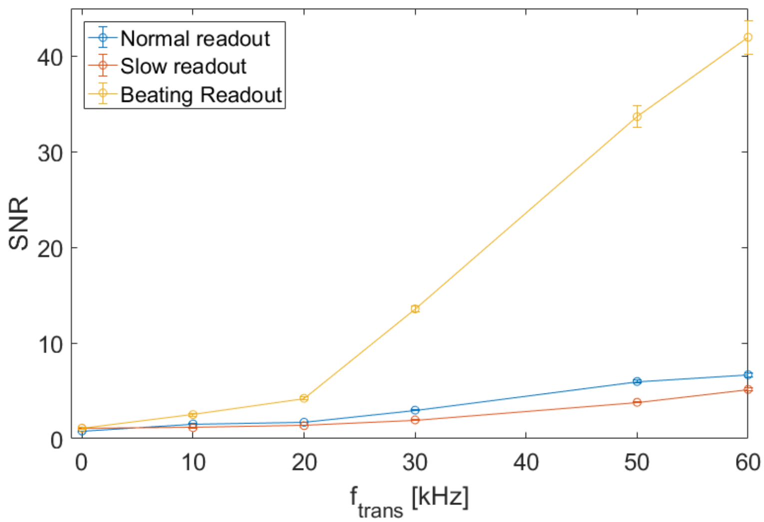

Figure 9: The signal to noise ratio (SNR) as a function of f_{trans} and arbitrarily varying readout rabi frequencies, f_{read}.

It can be seen that the beating readout method exceeds the other methods for high f_{trans}. Nevertheless it is still only slightly better than the scanning methods at low f_{trans}. Since the slow readout method did not show any increase in SNR as compared to the normal readout method further investigation into it was not performed. Instead focus was put into the superposition beating method.

4.2 Superposition beating tests for various f_{read}

Varying the readout rabi frequency, f_{read}, for different peak sizes, f_{trans}, constitutes the bulk of this section. Figure 10 shows some readouts for different peak sizes at an $\omega_{beat} = 1$MHz.

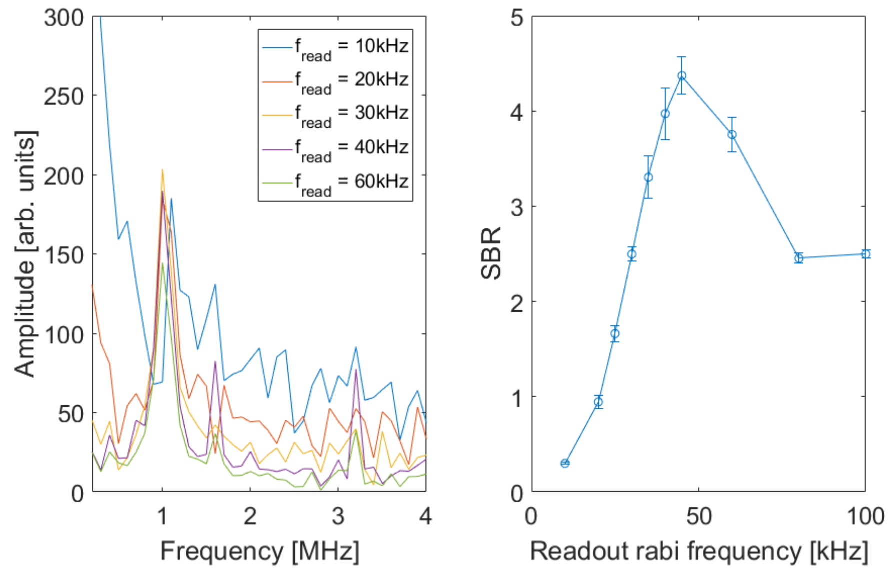

(a) $f_{trans} = 20$kHz

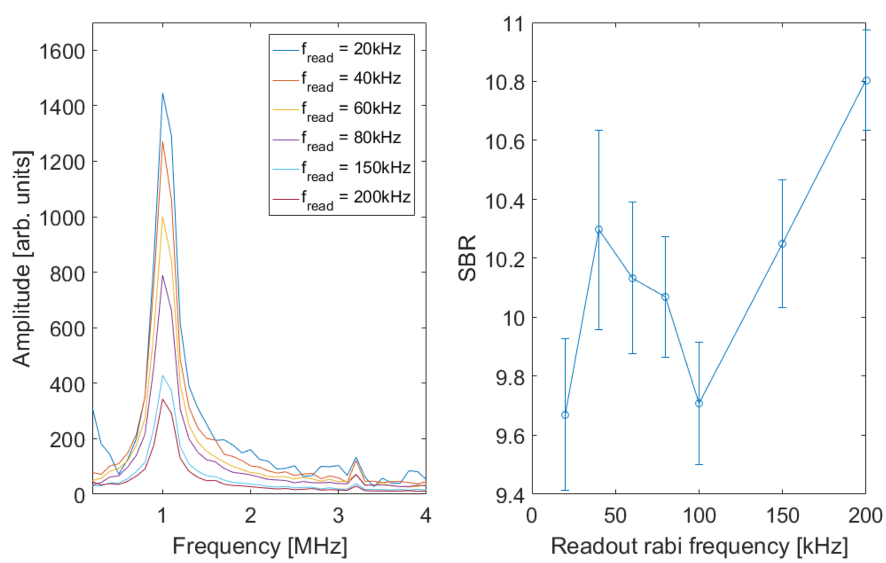

(b) $f_{trans} = 50$kHz

Figure 10: The Fourier transform of the signal and the corresponding SBR for different readout rabi frequencies f_{read}. The SBR is calculated using the first method in section 2.6.

Harmonic structure

It can be seen from the leftmost plots of figure 10(a) and 10(b), that for each f_{trans} a harmonic structure with a 1.6MHz recurrence arises. This structure has constant amplitude for varying f_{trans}. There is no possible way of obtaining the values at which these peaks are situated using the energy level diagram of figure 2. Additionally, the hole burning protocol takes care of keeping the pit empty. Consequently, these peaks were assumed to arise from systematic equipment related errors.

For subsequent investigations, in order to strike a compromise between the bandwidth of the detector and staying away from this structure, ω_{beat} is chosen to be 2.4MHz.

1/f noise

As is especially clear in figure 10(a), there is a large source of 1/f noise at the beginning of the Fourier spectrum that grows with lower f_{read}. The cause is the saturation of the detectors after the superposition has been established. Since there is no waiting time between the superposition pulse and the readout pulse, the detectors must desaturate while measuring the beating signal. As shown in figure 11, this desaturation can be approximated with a line of equation $I = -at$ with a positive. The Fourier transform of such a line recreates the observed 1/f structure, with the property that as a becomes larger, the 1/f noise spreads out further.

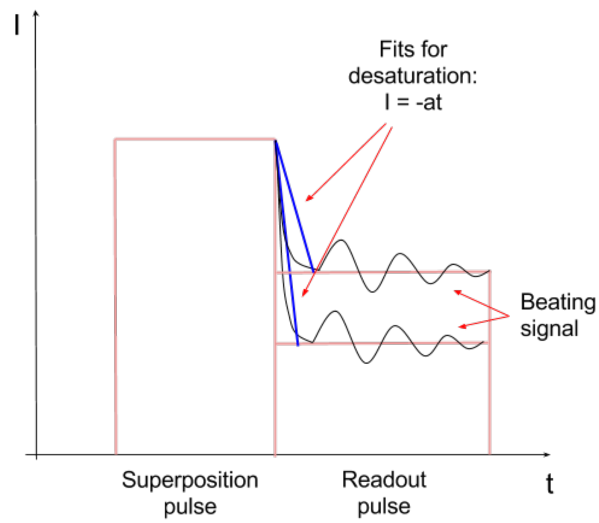

Figure 11: The pulse sequence (red) and the signal (black) as seen on the oscilloscope when the beating measurement is performed. The two readout pulses correspond to two different f_{read}.

As seen by the lower readout pulse of figure 11, the mean of the beating signal is low at low f_{read}, in other words the distance in intensity between the superposition and readout pulse is far. Hence the line that connects the two will be steeper. This is in exact accordance to all the Fourier spectra so far seen. Solutions include either inserting a wait pulse to the protocol or, as will be done for the remaining investigations, fitting a line (the blue lines in figure 11) and subtracting it from the signal before the Fourier transform is performed.

Signal to Background ratio

This first version of the signal to background ratio is sensitive to the choice of signal and background noise domain. It also has a very erratic nature, as seen in the second plots of figures 10(a) and 10(b). Furthermore the signal does not always increase with f_{read} as established by the principles of heterodyne detection. This will be addressed after the more robust SBR has been introduced.

4.3 Superposition beating tests at $\omega_{beat} = 2.4$MHz

Tests using the second more robust version of the SBR in section 2.6 and moving ω_{beat} to 2.4MHz are presented in this section.

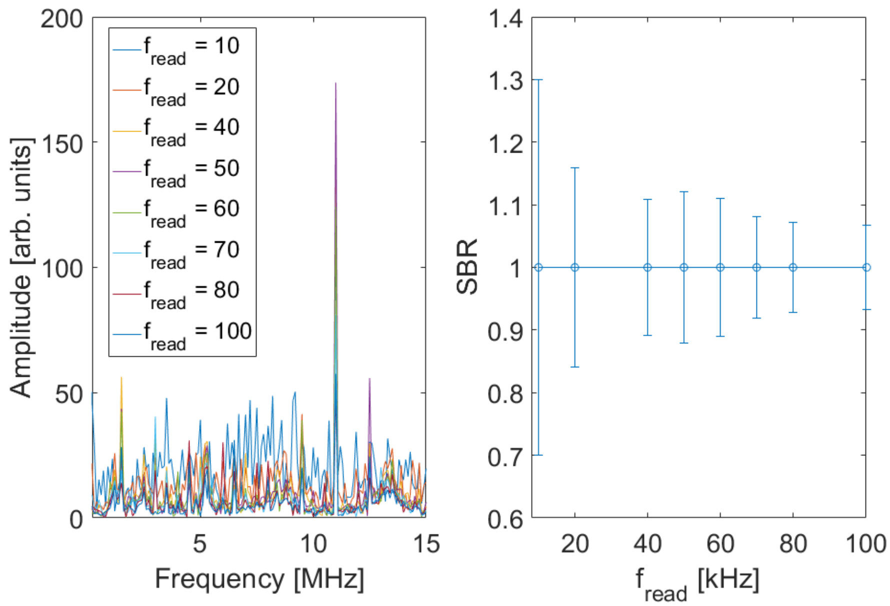

(a) $f_{trans} = 0$kHz

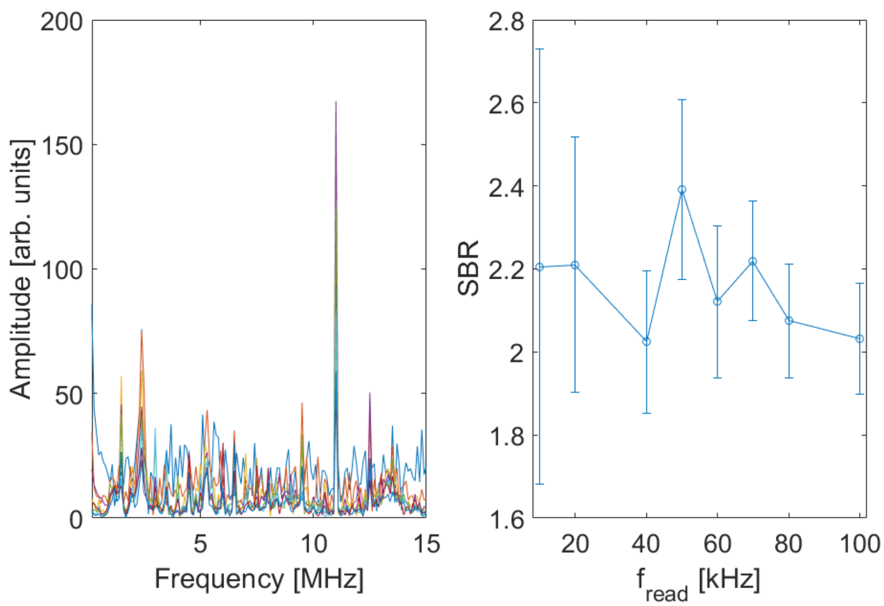

(b) $f_{trans} = 12$kHz

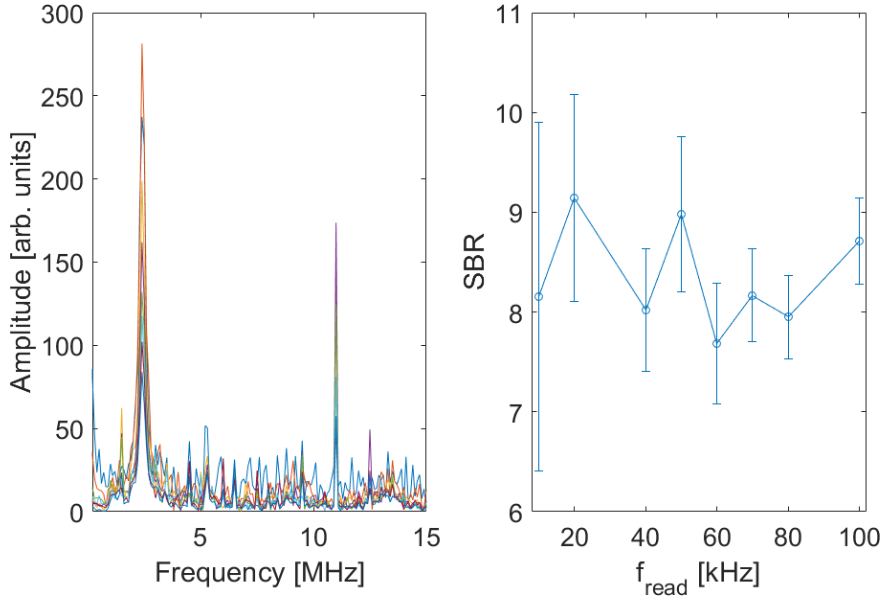

(c) $f_{trans} = 20$kHz

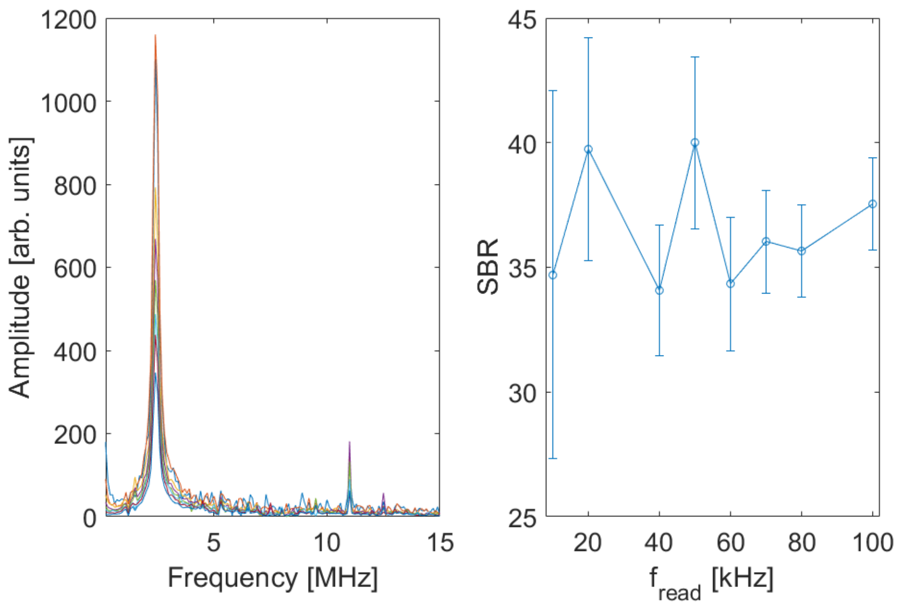

(d) $f_{trans} = 40$kHz

Figure 12: Each subfigure consists of, to the left: the Fourier transform of the raw signal divided by the reference, and to the right: the SBR for different readout rabi frequencies, f_{read}. They are equivalent to figure 10 except with a different f_{beat} and a change in the calculation of the SBR. The legend of (d) is the same for all plots (a)-(d)

The peaks of the left plots of figure 12(a)-(d) are clearer compared to those of figure 10 since they do not overlap with any harmonics and lack the strong 1/f noise. It is interesting to compare figure 12(c) with figure 10(a). A clear trend of improvement of the signal to background ratio can be observed.

The structure of the SBR

As previously mentioned and shown in equation 12, as one increases the electric field of the readout signal, heterodyne detection dictates that the signal intensity increases. The opposite is seen in figures 12(a)-(d). This is due to the division of the full signal by the reference which, as shown in equation 13, leads to an inversely proportional relation between the signal amplitude and readout rabi frequency:

$$\text{Full Signal} = \frac{I}{I_{ref}} \propto \frac{f_{read}}{f_{read}^2} = f_{read}^{-1}. \tag{13}$$

Equation 14 is a calculation of the SBR with the experimental data, characterized by equation 13:

$$\text{SBR} = \frac{\text{Signal}}{\text{Background}} \propto \frac{f_{read}^{-1}}{cf_{read}^{-1}} = \frac{1}{c} \tag{14}$$

for some constant c. This recreates the experimentally observed constant trend of the SBR with respect to f_{read} seen in figures 12(a)-(d).

Affecting the superposition

This constant trend does not go on indefinitely since as f_{read} increases, the superposition will be affected, causing it to send out less light. This means that at some point the signal will decrease while the background stays unchanged. Figures 13(a) and 13(b) give a quantitative grasp of this effect by showing the results of Bloch simulations with the same parameters as the f_{read} pulses, i.e., $\delta = -2.4$MHz and $\Omega = 2\pi f_{read}$.

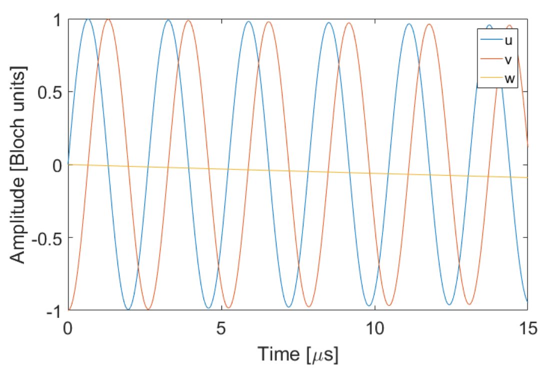

(a) $f_{read} = 0$kHz

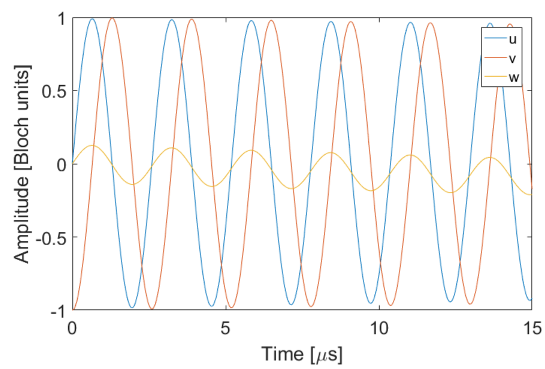

(b) $f_{read} = 50$kHz

Figure 13: Bloch simulations to visualize the effect the readout pulse has on the established superposition with state vector $\vec{R} = (0, -1, 0)$. Identical parameters to the experiments are used for these simulations. The slope of w is caused by the $\sim 160\mu$s lifetime of the superposition state.

Figure 14 provides an understanding of the results of figure 13. At non-zero detuning, as soon as there is any Rabi frequency, the precession of $\vec{R}$ around $\vec{W}$ will not follow the equator. This precession can be seen as the dotted circles of figure 14. The angles between the dotted planes and the equatorial plane of the Bloch sphere is what causes the oscillation in w. Recall from section 2.3 that $\vec{W} = (-\Omega_{re}, \Omega_{im}, -\delta)$. Hence when $\Omega << \delta$, the driving vector $\vec{W}$ will point mainly along the z-axis. Defining an angle θ as in figure 14, the $\Omega << \delta$ condition will lead to the approximation that $\sin\theta \approx \theta$. Since $\sin\theta \propto \Omega$, this means that the amplitude of the oscillations in w will vary linearly with Ω.

If the w component of the state vector $\vec{R}$ is nonzero, the equatorial projection will be less than 1 (see figure 3), meaning that a lower intensity of coherent light will be emitted. Therefore, the oscillation of w in figure 13(b), will cause the signal to decrease with f_{read}.

For figures 12(a)-(d), f_{read} is still in the $\Omega << \delta$ regime, so the SBR will not decrease visibly but look like it follows equation 14. However as soon as one leaves this regime the faster loss of coherently emitted light will cause a visible decrease in the signal to background ratio.

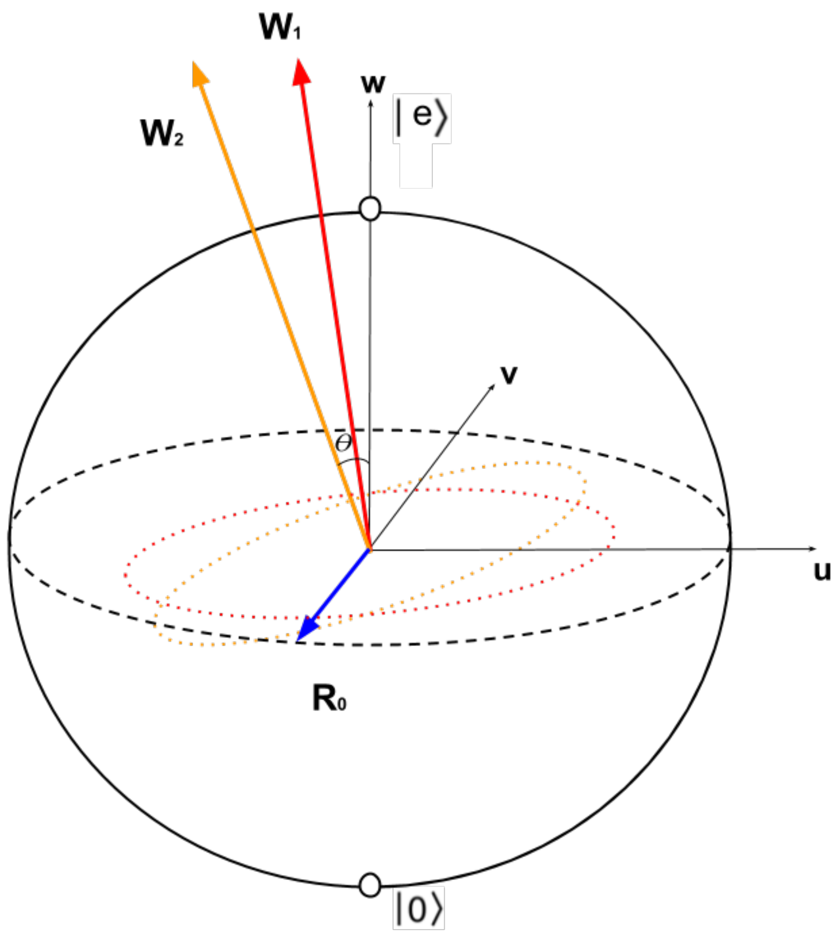

Figure 14: A visualization of how the initial superposition state given by $\vec{R}_0$ will move around the Bloch sphere with different driving vectors, $\vec{W}_1$ and $\vec{W}_2$. Both $\vec{W}_1$ and $\vec{W}_2$ have the same detuning, however $\vec{W}_1$ has a lower rabi frequency. The arrow sizes are not to scale.

SBR against f_{trans}

By compiling values from every plot of the form of figure 12, figure 15 gives a clear view of how the signal to background ratio varies with f_{trans}.

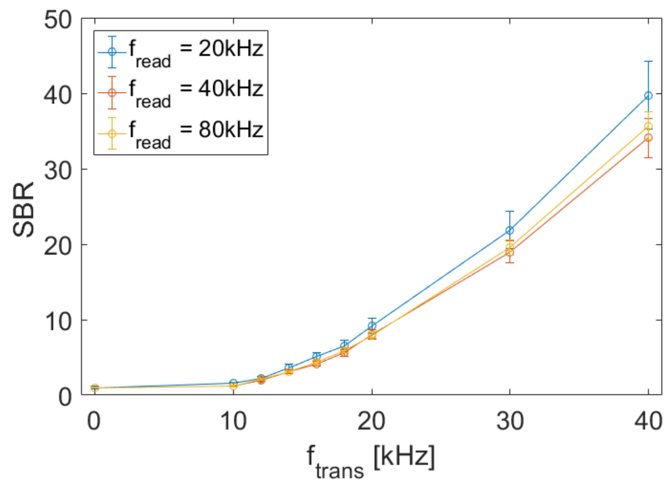

Figure 15: The SBR as a function of f_{trans} for various f_{read}. These values are directly extracted from plots of the same kind as figure 12.

As is expected, this line follows the shape that the beginning of a sechyp pulse has with respect to the population, as seen by the yellow line of figure 4(b). The advantage with this SBR calculation as compared to previous methods is that the shape of these curves is robust against the intensity of the readout signal. This is something that had been lacking for previous experiments.

4.4 f_{trans} as a measure of population size

For further work with this method it is important to characterize f_{trans} and see if it really is a good measure of the population size in the $|0\rangle$ state. This was done by performing Bloch simulations with pulses of the form of equation 6, where Ω_0 is $2\pi f_{trans}$.

Simulations

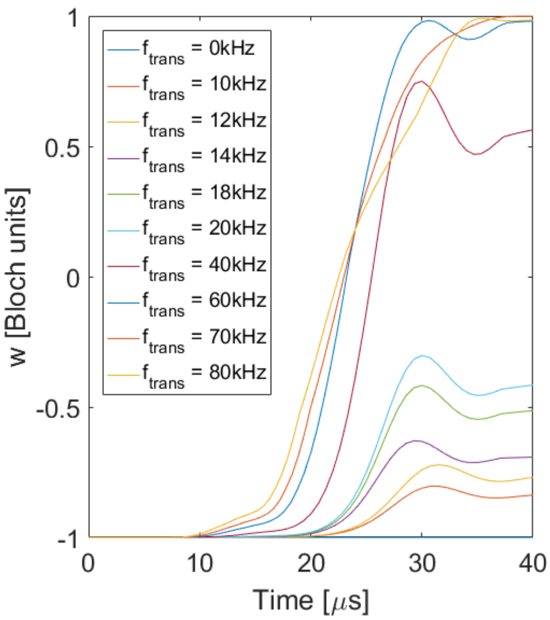

(a) The w component

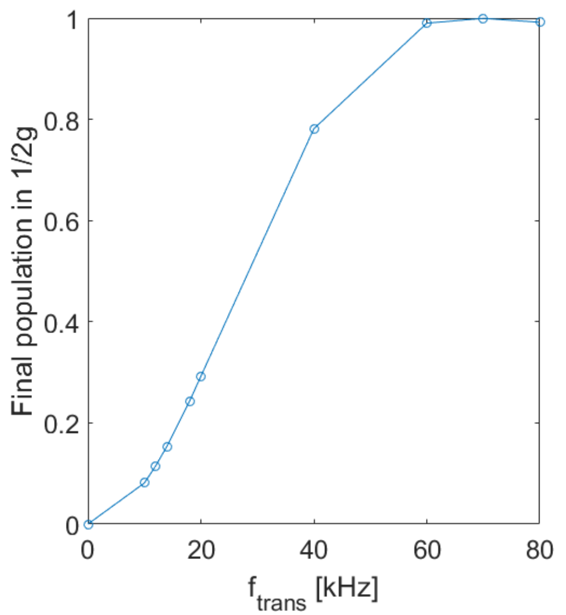

(b) The final population in 1/2g, interpolated from figure (a) at time 40μs

Figure 16: Results of Bloch simulations with the same parameters as the transfer pulse moving a population from a ground state to an excited state.

In accordance with figure 4(b) and the interchangeability between rabi frequency and pulse duration, figure 16 shows how increasing the rabi frequency will cause the final population in the excited state to follow this characteristic sechyp transfer trend. However the high transfer rabi frequencies will cause problems, since they all lead to a full population transfer in the simulations while the experimentally observed peaks still grow (this can be seen when using the normal readout method for $f_{trans} > 60$kHz). This discrepancy between the population size and the rabi frequency is caused by the Bloch simulations which fail to take into account the drop in rabi frequency due to the interaction between the electric field of the pulse and the crystal structure. Maxwell Bloch equations take care of this by adding extra terms to compensate for this interaction. Nonetheless the values of figure 16 will be true for the first "optical layers" of the crystal, where the laser intensity has not yet dropped too much. This fact will allow us to draw qualitative conclusions even though Maxwell Bloch simulations are beyond the scope of this thesis.

4.5 Different transitions

In order to optimize the signal, the use of the different oscillator strengths of various transitions was also considered. During this investigation the 50/50 superposition was set between the 1/2 ground state and the three excited states respectively. Figure 17 is the Fourier transform of the beating signal for each transition and for two different population sizes. It can be seen that the peak height grows with the oscillator strength, i.e., the $|1/2g\rangle + |1/2e\rangle$ state gives a higher signal than the $|1/2g\rangle + |3/2e\rangle$ which in turn gives a higher signal than the $|1/2g\rangle + |5/2e\rangle$ state. This follows the trend given by equation 10.

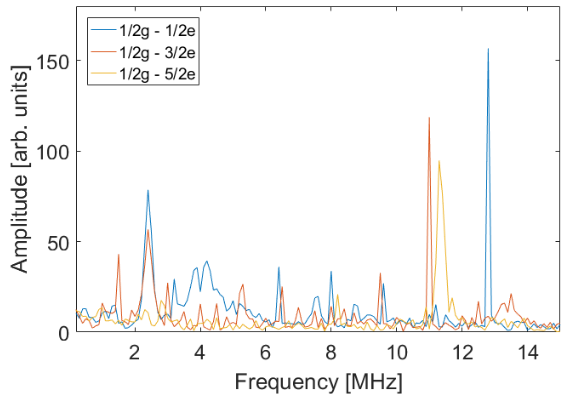

(a) $f_{trans} = 14\text{kHz}$

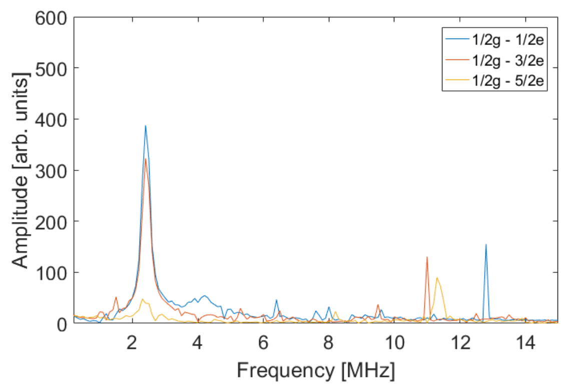

(b) $f_{trans} = 30\text{kHz}$

Figure 17: The Fourier transformed data for the readout when performed on different transitions.

Even though the peak sizes follow this trend, this might not be true for the SBR since the background signals are different for each superposition state (most clearly seen by the separation of the three peaks around 11MHz). The lack of measurements at $f_{trans} = 0\text{kHz}$ means that this investigation could not be performed.

Saturation of the detectors

Even though the peak sizes should follow equation 10, this dependence was not observed in the measurements. This is most probably due to the saturation of the detectors. For example since the oscillator strength of the $1/2g - 5/2e$ transition is low, the high rabi frequency of the superposition pulse saturated the detectors causing the beating signal to be measured much later in time. This delay would have caused a loss in fluorescent light due to the decay of the state.

5 Discussion

5.1 The constant nature of the SBR

The constant nature of the SBR means that these measurements will be robust against intensity fluctuations of the laser pulse. Even though this robustness exists, it is beneficial to go to higher f_{read}, since when the relative shot noise is high it can be difficult to distinguish between two populations, see the large error bars on the SBR plots of figure 15. In fact the error bars for $f_{read} = 20$kHz in figure 15 overlap for a difference in f_{trans} that is lower than 2kHz. In contrast they only overlap for a difference smaller than 0.8kHz when $f_{read} = 80$kHz.

This benefit of going to higher f_{read} in order to obtain higher population resolution does not go on indefinitely, since at some point the superposition will be affected too much. As already discussed in section 4.3, the slow linear way that the readout pulse affects the superposition depends on the fact that $\Omega << \delta$. Therefore when this regime is left, the SBR will decrease in a faster manner. In conclusion there is some optimal f_{read} where the SBR is still high and the error bars are at their smallest. It is unclear if this point has been reached during these experiments.

Finding this optimum is an important investigation to do when considering future CNOT gate experiments. So far it seems like the size of the ensembles that we would like to entangle are minuscule, hence the relevant signals will be very slight peak differences in the readouts. Therefore good resolution could be the difference between proving that two qubits have been entangled or not.

5.2 Visibility of small populations

In principal the percentage of the population that is lost in background noise is equal to the fraction between the noise and the peak. Hence, as has been continually stated throughout the thesis, a higher SBR indeed means that more of the population is visible. As a matter of fact, in the initial experiments, 16kHz was chosen as the smallest peak that could be discerned by eye using the normal readout method. Even though the lack of Maxwell Bloch simulations makes figure 16 quantitatively incorrect at deeper optical layers of the crystal, at least in the surface layers its value of around 12% at 16kHz hints towards a significant population that goes undetected when using the normal readout method. Figure 12(b) along with figure 16 shows that a population lower than 7% can be seen with the superposition beating method.

5.3 Varying SBR domain

As already mentioned, the absolute size of the recurring peaks in the spectra of figure 12 stays constant with f_{trans}. For example the peak at 11MHz keeps an amplitude of around 150. Therefore increasing the SBR by increasing the domain over which it is calculated is a possibility. In this way one could include anything that grows with f_{trans} such as the less important harmonic structure of the signal at $n \cdot 2.4$MHz, creating the possibility to see smaller peaks. The effect of these changes can be seen in figure 18 and the subsequent calculations.

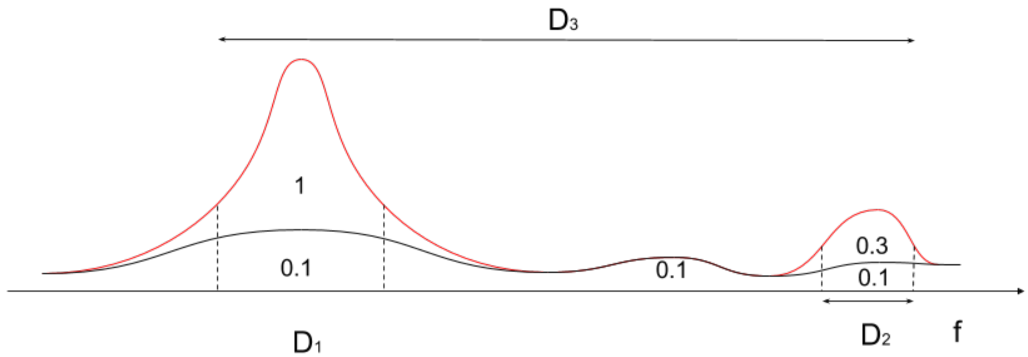

Figure 18: A visualization of how the signal to background ratio will vary due to the choice of domains D_1, D_2 or D_3. The red and black line corresponds to signal and background respectively.

The calculation of SBRs for the four domains D_1, D_2, D_3 and $D_1 + D_2$ gives:

$$\mathrm{SBR}_{D_1} = \frac{1}{0.1} = 10$$

$$\mathrm{SBR}_{D_2} = \frac{0.3}{0.1} = 3$$

$$\mathrm{SBR}_{D_3} = \frac{1 + 0.1 + 0.3}{0.1 + 0.1 + 0.1} = 4.3$$

$$\mathrm{SBR}_{D_1+D_2} = \frac{1 + 0.3}{0.1 + 0.1} = 6.5$$

Due to the division between signal and background we see that the D_1 domain gives the best SBR while the full D_3 domain gives the worst. Following this idea the SBR should be maximized when only the peak value is included. However fluctuations in the background will cause the error of this SBR to be large, so a trade off between small error and large SBR needs to be investigated. From the plots of figure 12 the chosen D_1 domain corresponds to a domain of ± 0.2MHz around the central frequency, or approximately the peak width. Investigations into other parts of the spectrum that grow with the peak size was beyond the scope of this thesis.

6 Conclusion

Investigations into three different readout methods, the normal and slow readout scan and the superposition beating method, were performed. It was immediately clear from our measurements the superposition beating method exceeded the other two for the detection of small peaks so a thorough characterization of this method was executed.

Comparing figure 12(a) with a corresponding figure for $f_{trans} = 10$kHz, the errorbars of the respective SBRs are on the verge of overlapping. Hence the lowest detected peak was 10kHz which, according to figure 16, corresponds to a population size of 8%. Furthermore at higher readout rabi frequencies, a peak resolution of 0.8kHz was achieved, which corresponds to a resolution of around 2 percentage points of the population. Note that upon comparison with figure 16 the percentage values are upper bounds due to the already discussed problems with normal Bloch simulations.

Due to a lack of measurements no conclusion in how the oscillator strength of the transition affects the signal to background ratio could be made. This is something that could be left for further work along with Maxwell Bloch simulations and CNOT gates.

All ideas and results presented in this thesis are general for any readout of ensembles that behave quantum mechanically. However the idea of working qubits has been taken into account throughout the work. For example the choice of using the standard deviation of the mean as error bars was made with the ulterior motive that many measurements would have to be made to determine the state of a qubit. All in all a robust method of detection has been thoroughly investigated and might one day detect entangled qubits.

References

[1] Andrew Steane. Quantum computing. *arXiv:quant-ph/9708022*, Aug 1997.

[2] Michael A. Nielsen and Isaac L. Chuang. *Quantum Computation and Quantum Information*. Cambridge University Press, Cambridge, UK, 10th anniversary edition, 2000.

[3] David P. DiVincenzo. The physical implementation of quantum computation. *arXiv:quant-ph/0002077*, Feb 2000.

[4] Lars Rippe, Mattias Nilsson, Stefan Kröll, Robert Klieber, and Dieter Suter. Experimental demonstration of efficient and selective population transfer and qubit distillation in a rare-earth-metal-ion-doped crystal. *Phys. Rev. A*, 71:062328, Jun 2005.

[5] Mattias Nilsson. *Coherent Interactions in Rare-Earth-Ion-Doped Crystals for Applications in Quantum Information Science*. PhD thesis, Lund University, 2005.

[6] C. J. Foot. *Atomic Physics*. Oxford University Press, New York, USA, 2nd edition, 2005.

[7] Smite-Meister. Bloch sphere. *Available at:* `https://commons.wikimedia.org/wiki/File:Bloch_sphere.svg`, Jan 2009.

[8] Sune Svanberg. *Atomic and Molecular Spectroscopyy: basic aspects and practical applications*. Springer-Verlag, Berlin, Germany, 4th edition, 1991.

[9] Quantum information group. LUND UNIVERSITY Division of Atomic Physics.

[10] Merkel D. Kristian Chang, Tiejun and Randall Babbitt. Recovery of spectral features readout with frequency chirped laser fields. *Phys. Rev. A*, 69:112931, 2005.